

NiO Hollow Spheres with Stable Capacity Retention and Enhanced Rate Capability for Lithium Ion Batteries

X. H. Huang*, J. B. Wu, Y. Lin, R. Q. Guo

College of Physics & Electronic Engineering, Taizhou University, Taizhou, 318000, China

*E-mail: drhuangxh@hotmail.com

Received: 6 December 2012 / Accepted: 29 December 2012 / Published: 1 February 2013

NiO hollow spheres are prepared by co-hydrolysis of nickel nitrate and tetraethyl orthosilicate (TEOS) in an ammonia solution and subsequent calcination and HF treatment processes. The microstructures and morphologies are characterized by means of X-ray diffraction (XRD), scanning electron microscopy (SEM) and transmission electron microscopy (TEM). As the anode materials for lithium-ion batteries, the electrochemical performances of NiO hollow spheres are studied by cyclic voltammetry (CV) and galvanostatic charge-discharge cycle tests. NiO hollow spheres show a well capacity retention and the charge capacity at the 40th cycle can reach 91.4% of the 1st cycle. Compared with the solid NiO spheres, the rate capability is also remarkably enhanced. The improved electrochemical performances are attributed to the hollow spherical structure of NiO.

Keywords: NiO, Hollow sphere, Anode, Lithium ion battery.

1. INTRODUCTION

As anode materials of lithium ion batteries, NiO and other 3d transition-metal oxides have been receiving considerable attention [1–13], due to their reversible capacities much higher than those of the traditional carbon based materials. However, similar to other 3d transition-metal oxides, NiO has not entered the commercial application of lithium ion batteries, because its high capacity can only be attained at low charging/discharging current densities. At high current densities, the capacity and cycling performance of NiO is relatively poor, which are mainly attributed to the poor electron conductivity and the slow Li⁺ diffusion in NiO materials.

To solve these problems, great efforts have been made to fabricate various nanostructured materials [14–18], which have significant advantages when used as electrode materials. Generally, nanostructured materials exhibit large interface of electrode/electrolyte and short diffusion pathway of Li⁺, both of which are very important to the high capacity and rate capability. Among these

nanostructures, hollow spheres are widely investigated [19–24]. For example, uniform hollow Fe_3O_4 spheres prepared by J. Zhang and coworkers deliver a reversible specific capacity of 870 mA h g^{-1} after 50 cycles [25]. Double-shelled Co_3O_4 hollow spheres prepared by X. Wang and coworkers exhibit a superior capacity of 866 mAh g^{-1} over 50 cycles [26]. These excellent performances are attributed to the hollow spherical structure. Besides the above advantages, the hollow spherical structure also has good buffering ability against the volume change and thus alleviates the pulverization, which is favorable for their cycling performance.

In the present work, we presented a new way to prepare NiO hollow spheres. The hollow spherical structure demonstrates a great enhancement on the capacity, cycling stability and rate capability, which was investigated in detail.

2. EXPERIMENTAL

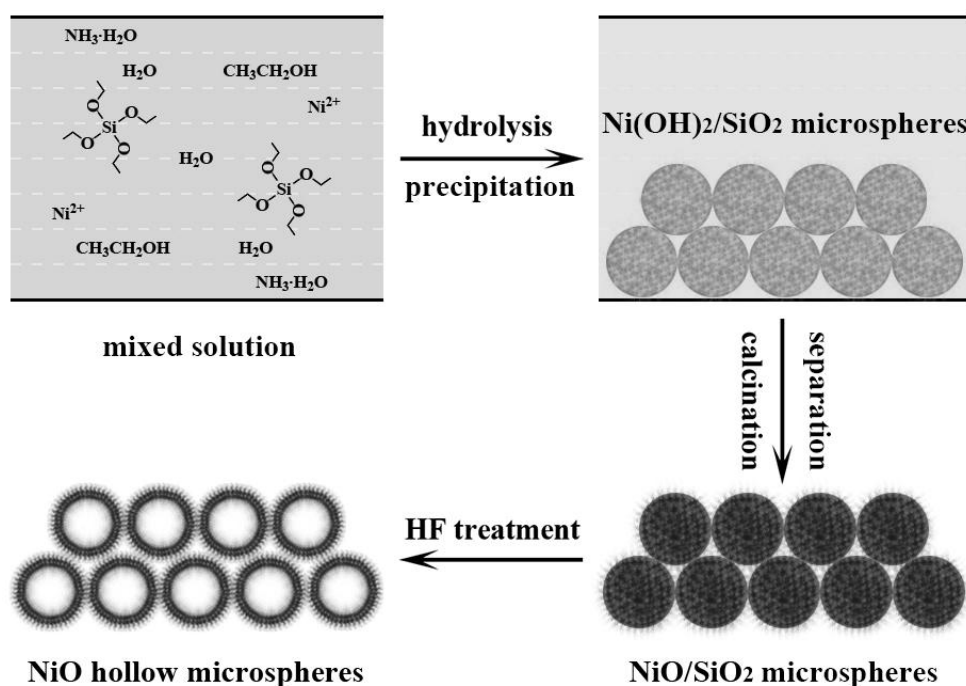


Figure 1. Schematic diagrams of the preparation process of NiO hollow spheres.

The preparation method of NiO hollow spheres is shown schematically in Figure 1. Firstly, 3.9 g nickel nitrate hexahydrate was dissolved into a mixed solution containing 20 mL absolute ethanol, 50 mL distilled water and 60 mL concentrated ammonia. Under intensely stirring, 4 g TEOS was injected slowly into the solution with a syringe. The stirring lasted for 36 h at room temperature. The precipitates were centrifuged, washed with distilled water and ethanol for several times, dried in a vacuum oven and calcined at $450 \text{ }^\circ\text{C}$ for 3 h. Then the sample was ultrasonically dispersed in a 0.5 wt% HF solution for 40 min to remove the hydrolyses of TEOS. Finally, NiO hollow spheres were obtained after drying.

The structure of the materials was characterized by means of X-ray diffraction (XRD, Bruker D8 advance; Cu K α radiation). The morphology was investigated by scanning electron microscopy (SEM, Hitachi S-4800) and transmission electron microscopy (TEM, JEOL JEM200CX).

The working electrode was prepared by a slurry-coating process. The slurry, containing NiO powder (80 wt%), acetylene black (12 wt%) and polyvinylidene fluoride (PVDF, 8 wt%) dissolved in *N*-methylpyrrolidinone (NMP), was pasted on the copper foil substrate. The working electrodes were then dried in vacuum at 100 °C for 12 h.

The working electrodes were assembled into CR2025 coin-type half cells for electrochemical investigations using pure lithium wafers as the counter electrodes, 1 mol L⁻¹ LiPF₆ in ethylene carbonate (EC) and dimethyl carbonate (DMC) (1:1 in weight) as the electrolyte, and polypropylene (PP) microporous film (Cellgard 2300) as the separator. The assembly process was performed in a dry argon-filled glove box (Mikrouna Super) where the concentrations of water and oxygen were controlled below 1 ppm.

The galvanostatic charge-discharge tests of the cells were conducted on a program-control battery test system (Land CT2001A) using different current densities between the cut-off voltages of 0.02–3.0 V at room temperature. Cyclic voltammetry (CV) tests were performed on an electrochemical workstation (CHI600D) with a sweep speed of 0.1 mV s⁻¹ in the potential range of 0–3 V.

3. RESULTS AND DISCUSSION

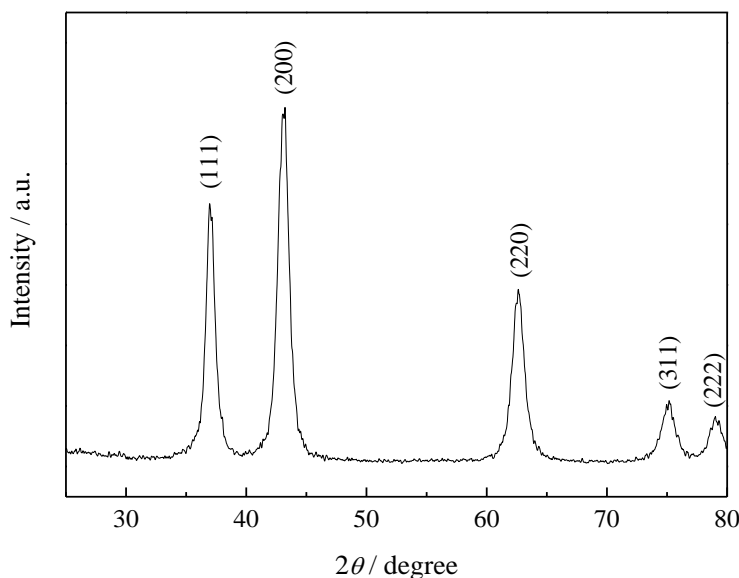


Figure 2. XRD pattern of the NiO hollow spheres.

Figure 2 presents the XRD pattern of the finally products. The pattern shows five diffraction peaks at 37.0, 43.3, 62.6, 75.2, 79.0°, which can be assigned to the (111), (200), (220), (311) and (222) reflections of cubic NiO, respectively, according to JCPDS No. 47-1049.

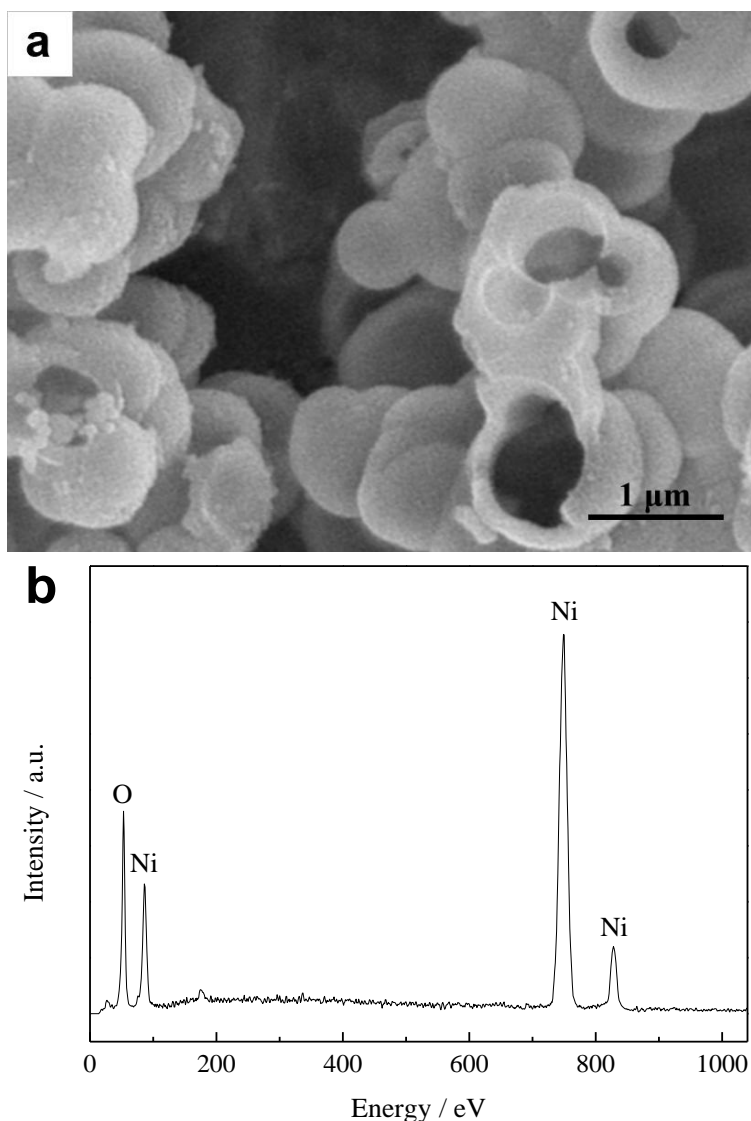


Figure 3. (a) SEM image of NiO hollow spheres and (b) the corresponding EDS pattern.

SEM images of the NiO sample are given in Figure 3. The sample shows a hollow spherical structure (Figure 3a), with diameters of about 1–1.5 μm and shell thicknesses of about 200 nm. EDS pattern (Figure 3b) indicates that, except Ni and O, no obvious impurity can be found. This suggests that the hydrolysis products of TEOS have been removed by HF completely and the residue is pure NiO.

The microstructure of NiO hollow spheres is also investigated by TEM (Figure 4). The sphere has a very clear hollow structure, and is assembled by many nanoparticles. The corresponding SAED pattern exhibits {111}, {200} and {220} diffraction rings of NiO, confirming that the NiO hollow spheres are polycrystalline.

CV test was performed between 0–3 V at a sweep speed of 0.1 mV s⁻¹ to investigate the electrochemical reactions towards Li. Figure 5 is the CV curves of the first three cycles. In the first cycle, it exhibits a strong cathodic peak at about 0.45 V. This peak is related to the first

electrochemical process of NiO, including the reduction of NiO to Ni and the formation of the solid electrolyte interface (SEI) layer.

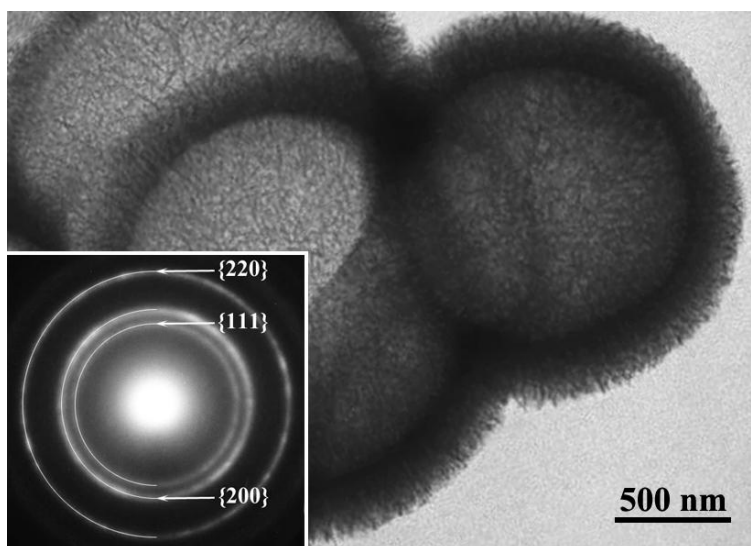


Figure 4. TEM analysis of NiO hollow spheres and the corresponding SAED pattern.

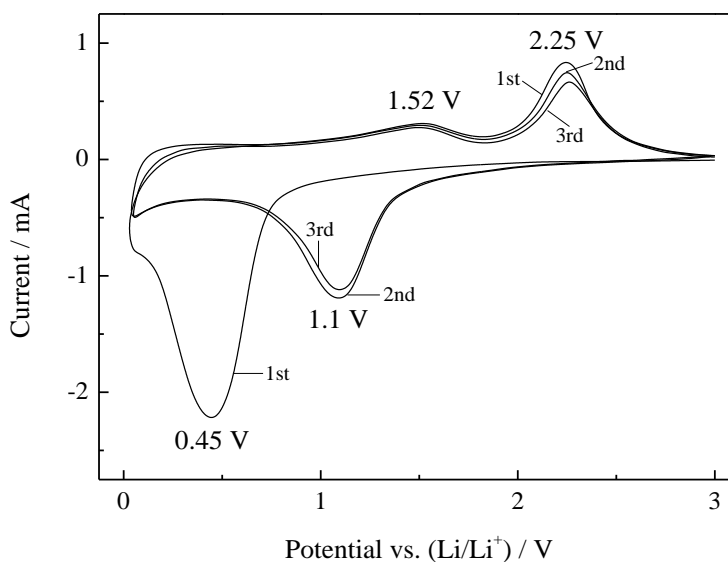


Figure 5. CV curves of NiO hollow spheres at a scanning rate of 0.1 mV s^{-1} .

The SEI layer is an organic-like layer, and consists of ethylene-oxide-based oligomers, LiF, Li_2CO_3 , and lithium alkyl carbonate (ROCO_2Li) [27]. The potentials of the two reactions are very close, so it exhibits a strong intensity. The first anodic scan shows two anodic peaks, which located at 1.52 and 2.25 V, respectively. The peak at 1.52 V is due to the partial decomposition of the SEI layer [1–4]. Another peak, at 2.25 V, is ascribed to the reoxidation process of Ni back to NiO. In the second cycle, the cathodic peak shifts to a higher potential at 1.1 V with decreased intensity, exhibiting a

smaller polarization. Moreover, it can be seen that since the second cycle, the electrochemical reactions are reversible.

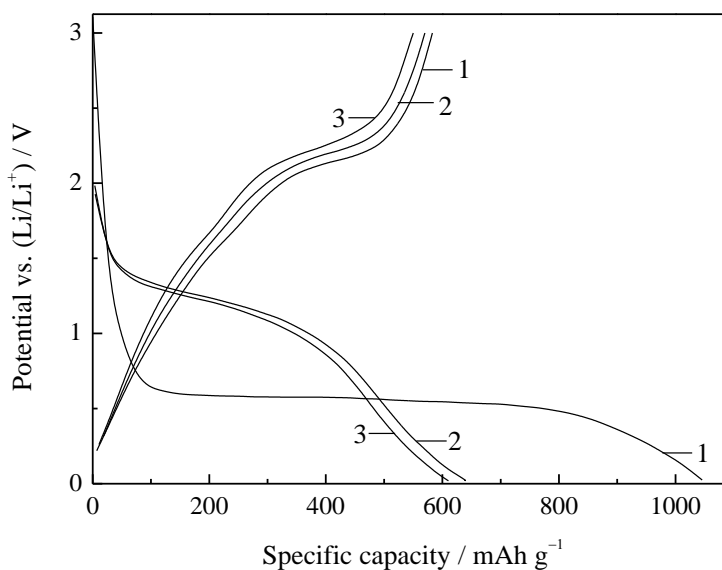


Figure 6. The first three galvanostatic discharge-charge cycle curves of NiO hollow spheres at the current density of 0.2 A g^{-1} .

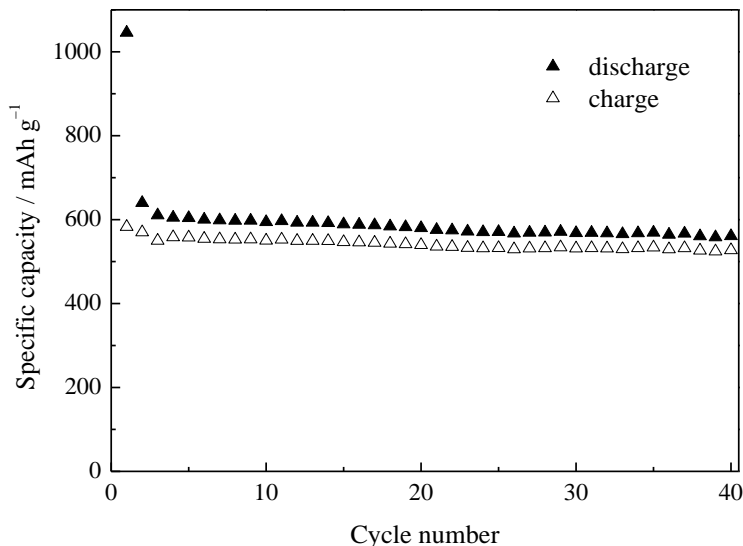


Figure 7. Cycling performance of NiO hollow spheres until 40 cycles.

The cells were galvanostatically discharge-charged repeatedly in order to investigate its capacity and cycling performance. Figure 6 is the discharge-charge curves of the first three cycles at the current density of 0.2 A g^{-1} . The first cycle is partially reversible, showing a first discharge capacity of 1045 mAh g^{-1} and a first charge capacity of 580 mAh g^{-1} . The theoretical capacity of NiO is 718 mAh g^{-1} , based on this electrochemical reaction equation ($\text{NiO} + 2\text{Li} \rightleftharpoons \text{Ni} + \text{Li}_2\text{O}$). The first

discharge capacity is much higher than the theoretical value, which is the common character of all the 3d transition-metal oxides. The extra capacity in the first discharge process mainly results from to the formation of SEI layer that consumes some Li. In the first discharge curve, there is a long plateau at about 0.5 V. While in the following charge process, no plateaus but two slopes at about 1.5 V and 2.3 V are found. In the second cycle, the discharge and charge capacities are 640 and 570 mAh g⁻¹, respectively, indicating a more reversible reaction. Smaller polarization is also observed, which is consistent with CV curves. In the third cycle, the shape of both discharge and charge curves are very similar to the second cycle except for some capacity fading. The discharge and charge capacities of 40 cycles are plotted in Figure 7. It can be seen that the capacities decrease slowly. The discharge and charge capacities of the 40th cycle are 560 and 530 mAh g⁻¹. It is calculated that 91.4% of the initial reversible capacity (charge capacity) remains after 40 cycles, much higher than those of many previous reported NiO spheres [20, 24, 28–31], indicating a stable capacity retention performance.

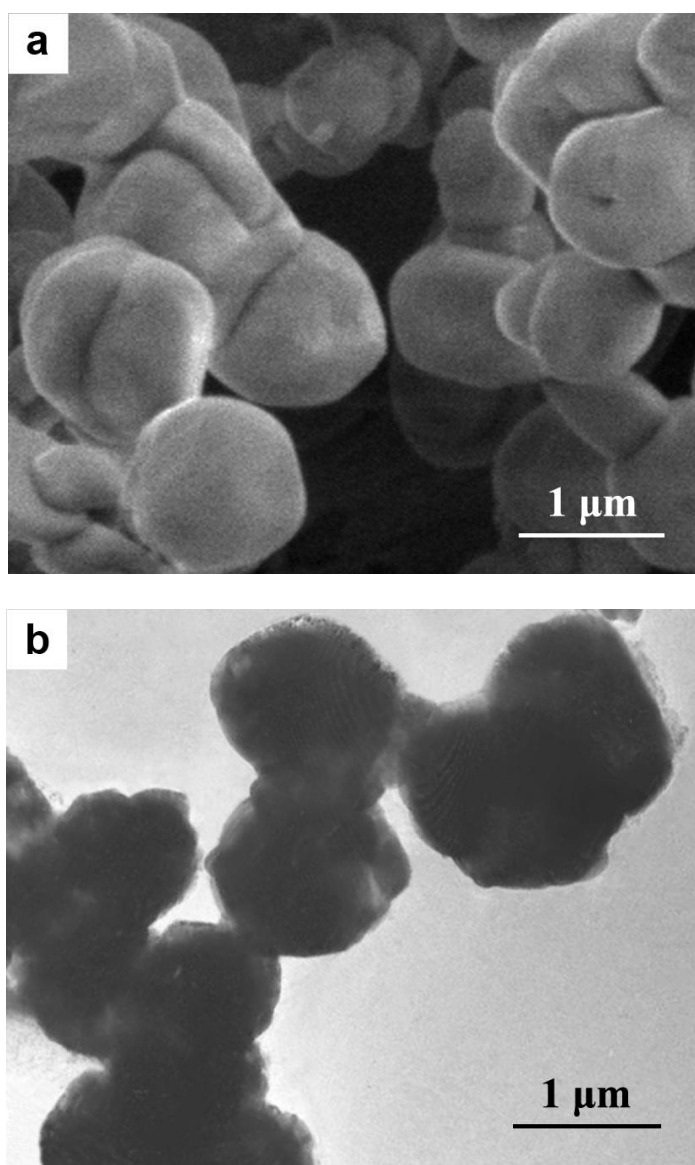


Figure 8. Morphology of the NiO solid spheres. (a) SEM image and (b) TEM image.

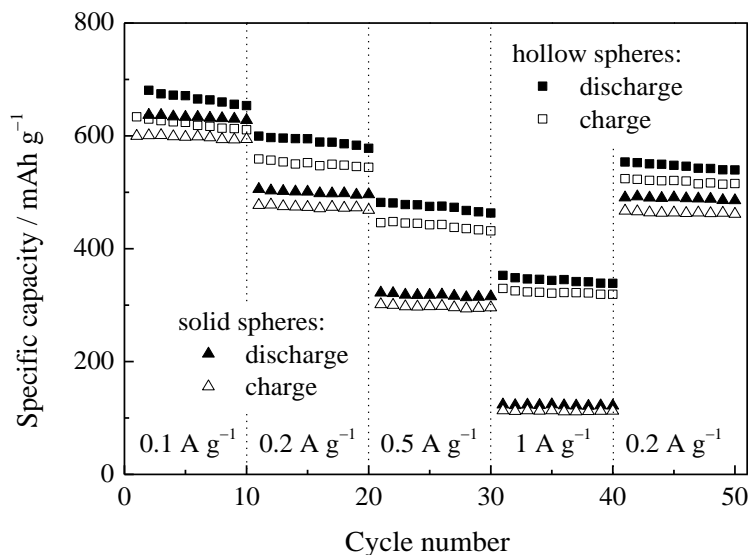


Figure 9. Comparison of rate capabilities of both hollow and solid NiO spheres at different current densities.

The rate capability of the NiO hollow spheres is also studied. To investigate the effect of hollow structure on the rate capability, solid NiO spheres are also prepared to make a comparison. Solid NiO spheres are synthesized by just heating the hollow NiO spheres at 650 °C for 2 h in air. During the heating process, NiO nanoparticles grow and assemble into solid spheres, which is confirmed by their SEM (Figure 8a) and TEM (Figure 8b) images. The cells made of these two materials were tested for 10 cycles at different current densities of 0.1, 0.2, 0.5, 1 and 0.2 A g⁻¹ in turn. The discharge and charge capacities of all stages are shown in Figure 9. Firstly, when the two electrodes are cycled at a low current density of 0.1 A g⁻¹, the hollow NiO spheres exhibit average discharge and charge capacities of about 670 and 620 mAh g⁻¹, while the solid NiO spheres exhibit smaller values of about 630 and 600 mAh g⁻¹. Subsequently, the current density is increased to 0.2, 0.5 and 1 A g⁻¹ in turn. The discharge capacities of hollow NiO spheres in each stage are about 590, 470, and 340 mAh g⁻¹, and the charge capacities are 550, 440 and 320 mAh g⁻¹, respectively. Solid NiO spheres show lower capacities at the same current densities, especially low at 0.5 and 1 A g⁻¹. Finally, the current density reduces to 0.2 A g⁻¹, the capacities of hollow NiO spheres recover to 550 and 520 mAh g⁻¹, also higher than that of the solid NiO spheres. Compared with our previous reported micro-sized NiO materials, the hollow spheres in the present work also exhibits better rate capability [19, 32].

The hollow structure is believed to play a vital role in the enhancement of the electrochemical performance of NiO. Larger specific surface area and easier infiltration into the electrolyte of two sides of the hollow spheres lead to a larger contact interface. These advantages enable more active particles to contact well with the electrolyte. The increase of reaction interface can reduce the current density per unit area and promotes the electrochemical reaction degree. The hollow structure also has an advantage of shortening the diffusion pathway of Li⁺ in the electrochemical reaction process. This facilitates the charge transfer and accelerates the electrochemical reactions. In addition, the void space in the hollow sphere offers a good buffering ability against the volume change, which alleviates the

pulverization and leads to a good cycling performance. As a result, NiO hollow spheres exhibit stable capacity retention and enhanced rate capability.

4. CONCLUSIONS

NiO hollow spheres are synthesized successfully by co-hydrolysis of nickel nitrate and tetraethyl orthosilicate (TEOS) in an ammonia solution and subsequent calcination and HF treatment processes. These hollow spheres have diameters of about 1–1.5 μm and shell thicknesses of about 200 nm. As anode materials for the lithium-ion batteries, NiO hollow spheres show a stable capacity retention and the charge capacity at the 40th cycle can reach 91.4% of the 1st cycle. Furthermore, compared with solid NiO spheres, the hollow spheres also exhibit an enhanced rate capability. The hollow structure plays an important role in the electrochemical performance, because it offers a larger specific surface area and larger contact interface, shorter diffusion pathways of Li^+ , and better accommodations of volume expansion of NiO in the electrochemical reaction processes.

ACKNOWLEDGEMENTS

The authors acknowledge the financial support from Zhejiang Provincial Natural Science Foundation of China (Grant No. LQ12E02004) and National Natural Science Foundation of China (Grant No. 51204116).

References

1. P. Poizot, S. Laruelle, S. Dupont and J-M. Tarascon, *Nature*, 407 (2000) 496.
2. S. Grugeon, S. Laruelle, R. Herrera-Urbina, L. Dupont, P. Poizot and J-M. Tarascon, *J. Electrochem. Soc.*, 148 (2001) A285.
3. P. Poizot, S. Laruelle, S. Grugeon and J.-M. Tarascon, *J. Electrochem. Soc.*, 149 (2002) A1212.
4. A. Débart, L. Dupont, P. Poizot, J-B. Leriche and J. M. Tarascon, *J. Electrochem. Soc.*, 148 (2001) A1266.
5. X. H. Huang, J. P. Tu, X. H. Xia, X. L. Wang, J. Y. Xiang, L. Zhang and Y. Zhou, *J. Power Sources*, 188 (2009) 588.
6. X. H. Huang, C. B. Wang, S. Y. Zhang and F. Zhou, *Electrochim. Acta*, 56 (2011) 6752.
7. X. H. Huang, J. P. Tu, X. H. Xia, X. L. Wang and J. Y. Xiang, *Electrochem. Commun.*, 10 (2008) 1288.
8. S. Y. Liu, J. Xie, Q. Pan, C. Y. Wu, G. S. Cao, T. J. Zhu and X. B. Zhao, *Int. J. Electrochem. Sci.*, 7 (2012) 354.
9. W. T. Song, J. Xie, S. Y. Liu, Y. X. Zheng, G. S. Cao, T. J. Zhu and X. B. Zhao, *Int. J. Electrochem. Sci.*, 7 (2012) 2164.
10. H. Xu, X. Chen, L. Chen, L. Li, L. Xu, J. Yang and Y. Qian, *Int. J. Electrochem. Sci.*, 7 (2012) 7976.
11. W. Kang, C. Zhao and Q. Shen, *Int. J. Electrochem. Sci.*, 7 (2012) 8194.
12. Y. Sun, X. Hu, W. Luo and Y. Huang, *J. Mater. Chem.*, 22 (2012) 13826.
13. Y. He, L. Huang, J. S. Cai, X. M. Zheng and S. G. Sun, *Electrochim. Acta*, 55 (2010) 1140.
14. F. S. Ke, L. Huang, B. Zhang, G. Z. Wei, L. J. Xue, J. T. Li and S. G. Sun, *Electrochim. Acta*, 78 (2012) 585.

15. Q. Q. Xiong, J. P. Tu, Y. Lu, J. Chen, Y. X. Yu, Y. Q. Qiao, X. L. Wang and C. D. Gu, *J. Phys. Chem. C*, 116 (2012) 6495.
16. H. S. Lim, B. Y. Jung, Y. K. Sun and K. D. Suh, *Electrochim. Acta*, 75 (2012) 123.
17. Y. F. Yuan, Y. B. Pei, J. Fang, H. L. Zhu, J. L. Yang and S. Y. Guo, *Mater. Lett.*, 91 (2013) 279.
18. Y. Deng, Q. Zhang, Z. Shi, L. Han, F. Peng and G. Chen, *Electrochim. Acta*, 76 (2012) 495.
19. X. H. Huang, J. P. Tu, C. Q. Zhang and F. Zhou, *Electrochim. Acta*, 55 (2010) 8981.
20. H. Qiao, N. Wu, F. Huang, Y. Cai and Q. Wei, *Mater. Lett.*, 64 (2010) 1022.
21. Y. Liu, C. Mi, L. Su and X. Zhang, *Electrochim. Acta*, 53 (2008) 2507.
22. W. Zhang, X. Wang, H. Zhou, J. Chen and X. Zhang, *J. Alloy. Compd.*, 521 (2012) 39.
23. Y. Deng, Q. Zhang, S. Tang, L. Zhang, S. Deng, Z. Shi and G. Chen, *Chem. Commun.*, 47 (2011) 6828.
24. C. Zhong, J. Z. Wang, S. L. Chou, K. Konstantinov, M. Rahman and H. K. Liu, *J. Appl. Electrochem.*, 40 (2010) 1415.
25. J. Zhang, Y. Yao, T. Huang and A. Yu, *Electrochim. Acta*, 78 (2012) 502.
26. X. Wang, X. L. Wu, Y. G. Guo, Y. Zhong, X. Cao, Y. Ma and J. Yao, *Adv. Funct. Mater.*, 20 (2010) 1680.
27. G. Gachot, S. Grugeon, M. Armand, S. Pilard, P. Guenot, J. M. Tarascon and S. Laruelle, *J. Power Sources*, 178 (2008) 409.
28. X. H. Huang, J. P. Tu, C. Q. Zhang, X. T. Chen, Y. F. Yuan and H. M. Wu, *Electrochim. Acta*, 52 (2007) 4177.
29. L. Liu, Y. Li, S. Yuan, M. Ge, M. Ren, C. Sun and Z. Zhou, *J. Phys. Chem. C*, 114 (2010) 251.
30. L. Yuan, Z. P. Guo, K. Konstantinov, P. Munroe and H. K. Liu, *Electrochem. Solid-State Lett.*, 9 (2006) A524.
31. Y. Yao, J. Zhang, Z. Wei and A. Yu, *Int. J. Electrochem. Sci.*, 7 (2012) 1433.
32. X. H. Huang, Y. F. Yuan, Z. Wang, S. Y. Zhang and F. Zhou, *J. Alloy. Compd.*, 509 (2011) 3425.